Optical and Quantum Electronics **24** *(1992) S273–S283*

AN INVITED PAPER

3-dimensional photonic band structure

E. YABLONOVITCH, T. J. GMITTER
Bell Communications Research, Navesink Research Center, Red Bank, NJ 07701-7040, USA

K. M. LEUNG
Dept. of Physics, Polytechnic University Brooklyn, NY 11201, USA

R. D. MEADE, A. M. RAPPE, K. D. BROMMER, J. D. JOANNOPOULOS
Dept. of Physics, MIT, Cambridge, MA 02139, USA

Received 24 June 1991; accepted 25 September 1991

Three-dimensionally periodic dielectric structures, (photonic crystals), possessing a forbidden gap for electromagnetic wave propagation, (a photonic bandgap), are now known. If the perfect 3-dimensional periodicity is broken by a local defect, then local electromagnetic modes can occur within the forbidden bandgap. The addition of extra dielectric material locally, inside the photonic crystal, produces 'donor' modes. Conversely, the local removal of dielectric material from the photonic crystal produces 'acceptor' modes. It will now be possible to make high-Q electromagnetic cavities of volume $\sim$ 1 cubic wavelength, for short wavelengths at which metallic cavities are useless. These new dielectric cavities can cover the range all the way from millimeter waves, down to ultraviolet wavelengths.

1. Introduction

There is an interesting analogy between electron waves in a crystal and light waves in a three-dimensionally periodic dielectric structure. Both should be described by band theory. The idea of photonic band structure [1, 2] is rapidly gaining acceptance [3–6]. The concepts of reciprocal space, Brillouin zones, dispersion relations, Bloch wave functions, Van Hove singularities, etc, are now being applied to optical waves.

Recently, some three dimensional topologies have been discovered [5, 7], in which a 'photonic bandgap' can open up. This is an energy band in which optical modes, spontaneous emission, and zero point fluctuations are all absent. Indeed, a photonic bandgap would be essentially ideal since optical dielectric response can be real and dissipationless.

In addition to the obvious applications in atomic physics, inhibited spontaneous emission can now begin to play a role in semiconductor and solid state electronics. If the photonic bandgap overlaps the electronic band edge, spontaneous electron-hole recombination is rigorously forbidden. In a semiconductor laser, this would lead to near unity quantum efficiency into the lasing mode. Photon number state squeezing [8] into that mode would be greatly enhanced.

0306–8919/92

efficiency into the lasing mode. Photon number state squeezing [8] into that mode would be greatly enhanced.

There have been a series of challenges in this field. The first was to show that a full 3-dimensional 'photonic bandgap' could actually exist in some type of dielectric structure. Then it was necessary to show that such a forbidden gap could be created in a micro-structure amenable to practical micro-fabrication. Now, practical methods of 'doping' the photonic crystal are being developed. Ultimately, a practical, electrically injected micro-laser incorporated inside the photonic crystal will have to be demonstrated.

At the outset of research on 3-d photonic band structure, it was realized [1] that a face-centred-cubic (f.c.c.) array in real space would produce the 'roundest' Brillouin zone in reciprocal space. Such a sphere-like Brillouin zone improves the prospects for a forbidden gap to have a common overlap all the way around its surface. But it was unclear what should be the real-space shape of the atoms in the f.c.c. array. The original suggestion [1] called for cubic atoms. Later, the first experimental effort [9] concentrated on dielectric spheres and on spherical voids in a dielectric background. The spherical void structure appeared to performed particularly well. During this period there was a search for that optimal 3-dimensional dielectric geometry, favoured by nature and by Maxwell's equations.

Around the same time, electronic band theorists began calculating photonic band structure. It rapidly became apparent that the familiar scalar wave band theory, so frequently used for electrons in solids, was in utter disagreement with experiment on photons [10–13]. Recently a full vector-wave band theory [3–5] became available, which not only agreed with experiments, it highlighted some discrepancies in experiment. Vector-wave band theory showed that spherical atomic symmetry produced a degeneracy between valence and conduction bands at the W-point of the Brillouin zone, allowing only a pseudogap, rather than a full photonic bandgap. Ho *et al.* [5] were the first to overcome this problem. They introduced diamond structure, which breaks the spherical symmetry by requiring 2 atoms per f.c.c. unit cell.,

More generally we find that the symmetry-induced degeneracy in f.c.c. lattices is lifted by making the atoms non-spherical. This has led to a practical, new, face-centred-cubic (f.c.c.) structure which simultaneously solves two of the outstanding problems in photonic band structure. (1) In this new geometry the atoms are non-spherical, lifting the degeneracy at the W-point of the Brillouin zone, and permitting a full photonic band gap rather than a pseudogap. (2) Furthermore, this fully 3-dimensional f.c.c. structure lends itself readily to micro-fabrication on the scale of optical wavelengths. It is created by simply drilling 3 sets of holes 35.26° off vertical into the top surface of a solid slab or wafer, as can be done for example by reactive ion etching. At refractive index $n \approx 3.6$, typical of semiconductors, the 3-d forbidden photonic bandgap width in this new structure is $\sim 20\%$ of its centre frequency. Calculations indicate that the gap remains open for refractive indices $n \geqslant 2$.

2. An f.c.c. photonic crystal with nonspherical atoms

The Wigner–Seitz (W–S) real-space-unit-cell of the f.c.c. lattice is a rhombic dodecahedron as shown in Fig. 1. The problem of creating an arbitrary f.c.c. dielectric structure reduces to the problem of filling the f.c.c. W–S unit-cell with an arbitrary spatial distribution of dielectric material. Real space is then filled by repeated translation and close-packing of the W–S unit cells. Scientific progress in this field has been marked by improved choices of how to fill the W–S unit cell with dielectric material. As already mentioned, early proposals called for cubic [1] atoms, then spherical atoms and spherical voids [8] to be inscribed inside the W–S unit cell.

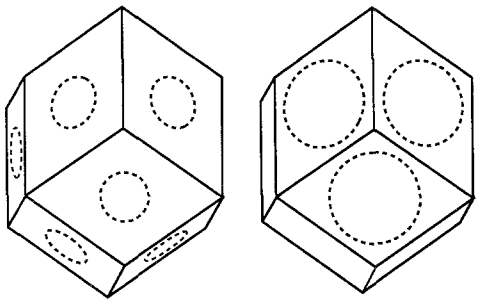

Figure 1 The Wigner–Seitz real-space-unit-cell of the f.c.c. lattice is a rhombic dodecahedron. In [8], slightly oversized spherical voids were inscribed into the unit cell, breaking through the faces, as illustrated by the dashed lines in (a). The current structure, shown in (b), is non-spherical. Cylindrical holes are drilled through the top 3 facets of the rhombic dodecahedron and exit through the bottom 3 facets. The resulting atoms are roughly cylindrical, and have a preferred axis, pointing up through the page.

Figure 1a shows a W–S unit cell filled by an over-sized spherical void, a structure which seemed to perform rather well in [9]. Since the spheres were slightly larger than close-packed, the voids broke through the surfaces of the W–S unit cell as indicated by the dashed circles on the faces of the rhombic dodecahedron in Fig. 1a. In [9] it was already pointed out that there was a symmetry-induced degeneracy at the W-point of the Brillouin zone in f.c.c. structures. There was a danger that the valence and conduction bands could touch at the degeneracy, closing the photonic bandgap. Based on the weight of experimental evidence however, it was argued [9] that the degeneracy had only caused adjacent conduction band levels to touch, permitting the gap to remain open. Vector-wave band theory, which has become quite successful recently [3–5], contradicted this. It showed that the degeneracy did indeed cause valence and conduction bands to touch at W, permitting only a pseudogap rather than a full photonic bandgap. Unfortunately, the finite-sized experimental sample in [9] allowed inadequate resolution to detect touching at isolated points on the Brillouin zone.

The degeneracy at W can be lifted by lowering the spherical symmetry of the atoms inside the W–S unit cell. We have made a close examination [14] of the degenerate wave-functions at W in the nearly-free-photon model, and learned that a distortion of the spherical atoms along the $\langle 111 \rangle$-direction will lift the degeneracy. The W–S unit cell in Fig. 1b has great merit for this purpose. Holes are drilled through the top 3 facets of the rhombic dodecahedron and then exit through the bottom 3 facets. The beauty of the structure in Fig. 1b is that a stacking of W–S unit cells results in straight holes which pass clearly through the entire 'photonic crystal'! The atoms are odd-shaped, roughly cylindrical voids centred in the W–S unit cell, with a preferred axis pointing to the top vertex.

An operational illustration of the construction which produces an f.c.c. 'crystal' of such W–S unit cells is shown in Fig. 2. A slab of material is covered by a mask containing a triangular array of holes. Three drilling operations are conducted through each hole, 35.26° off normal incidence and spread out 120° on the azimuth. The resulting criss-cross of holes below the surface of the slab produces a fully 3-dimensional periodic f.c.c. structure, with W–S unit cells given by Fig. 1b. The drilling can be done by a real drill for microwave work, or by reactive ion etching to create an f.c.c. structure at optical wavelengths. We have fabricated such 'crystals' in the microwave region by direct drilling into a commercial, low-loss, dielectric material, Emerson & Cumming Stycast-12. Its microwave refractive index, $n \approx 3.6$, is meant to correspond to that of the common semiconductors, Si, GaAs, etc. By simply scaling down the dimensions, this structure can be employed equally well at optical wavelengths. In this paper we will present the measured and calculated, ω versus k, dispersion relations for this new photonic crystal.

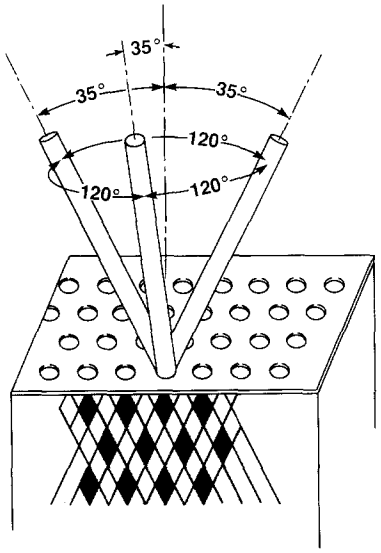

Figure 2 The method of constructing an f.c.c. lattice of the Wigner–Seitz cells as shown in Fig. 1b. A slab of material is covered by a mask consisting of a triangular array of holes. Each hole is drilled through three times, at an angle 35.26° away from normal, and spread out 120° on the azimuth. The resulting criss-cross of holes below the surface of the slab, suggested by the cross-hatching shown here, produces a fully 3-d periodic f.c.c. structure, with unit cells as given by Fig. 1b. The drilling can be done by a real drill bit for microwave work, or by reactive ion etching to create an f.c.c. structure at optical wavelengths.

The diamond symmetry of Ho, Chan and Soukoulis [5] can be created by supplementing the operations of Fig. 2 with three additional drilling operations, making a total of six drilling directions. These three new drilling directions, 120° apart, would all lie within the plane of the slab. Therefore they are somewhat difficult to implement experimentally. The six drilling directions correspond to the six inequivalent $\langle 110 \rangle$ channelling holes in diamond structure.

We have experimentally surveyed three f.c.c. structures, drilled in accordance with Fig. 2, to different ratios d/a of hole diameter d to f.c.c. unit cube length a: $d/a = 0.361$, 0.433, and 0.469. The removed volume fraction was approximately 62%, 70%, and 78% in the three cases, respectively. The 78% empty structure had the largest forbidden gap in this set and in this paper we will present results on that structure only. We believe 78% is near the optimal volume fraction for this f.c.c. geometry.

Our procedure is similar to the one we used in [9], except that our dynamic range was improved by using an HP-8510 network analyser for all the measurements. The experimental aim is to fully explore all 4π steradians in reciprocal space, while scanning frequency. The valence band edge frequency is defined by a sudden drop in microwave transmission, while the conduction band edge is defined by the frequency at which the transmitted signal recovers. Conservation of wave vector momentum parallel to the slab entry face determines the band edge position along the surface of the Brillouin zone. Since there are two polarizations, we can usually determine the two valence band edges and two of the conduction bands.

Sometimes the coupling of external plane waves to internal Bloch waves is poor, and the experiment can miss one of the conduction band edges, as happened in [9]. Finite sample size limits the useable dynamic range, exacerbating the weak coupling problem. Therefore it is important to back up the measurements with numerical calculations, which we have done as follows. The scalar dielectric constant distribution in Fig. 1 is expanded as a Fourier series in reciprocal space, while Maxwell's equations are expanded [3] as vector plane waves. The eigenvalues converge after a few hundred plane waves are summed in the expansion.

In spite of the non-spherical atoms of Fig. 1b, the Brillouin zone (BZ) is identical to the standard f.c.c. BZ shown in textbooks. Nevertheless, we have chosen an unusual perspective

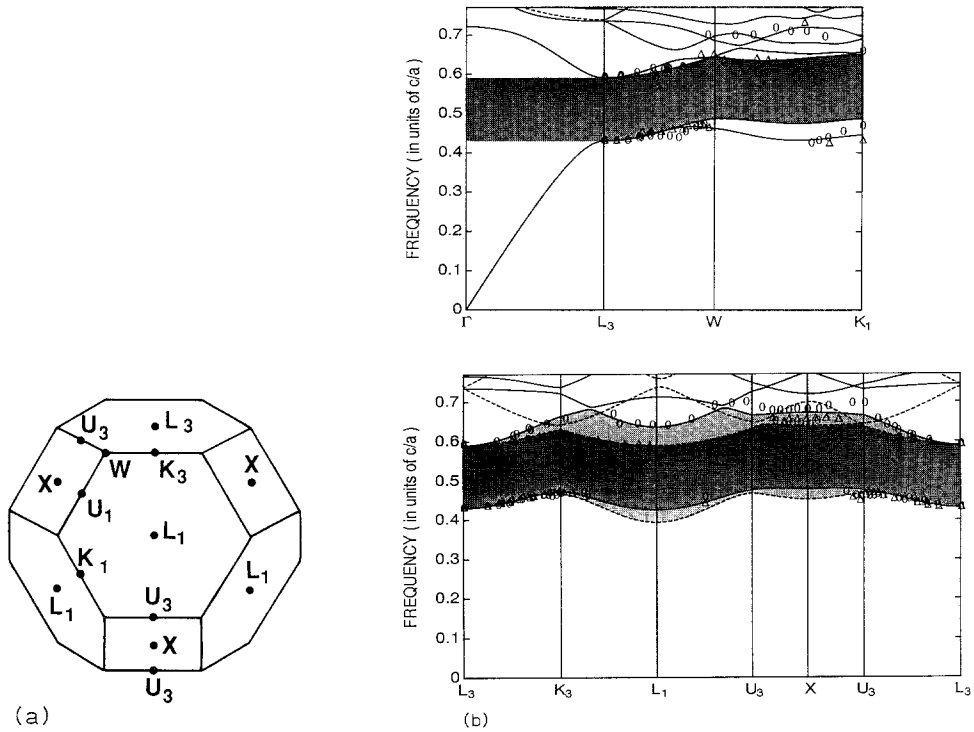

Figure 3 (a) The Brillouin zone of an f.c.c. structure incorporating non-spherical atoms, as in Fig. 1b. Since the space lattice is not distorted, this is simply the standard f.c.c. Brillouin zone lying on a hexagonal face rather than the usual cubic face. Only the L-points on the top and bottom hexagons are three-fold symmetry axes. Therefore they are labeled L_3. The L-points on the other six hexagons are labeled L_1. The U_3-K_3 points are equivalent since they are reciprocal lattice vector apart. Likewise the U_1-K_1 points are equivalent. (b) Frequency versus wave-vector, ω versus k, dispersion along the surfce of the Brillouin zone shown in 3a, where c/a is the speed of light divided by the f.c.c. cube length. The ovals and triangles are the experimental points for s and p polarization respectively. The solid and dashed lines are the calculations for s and p polarization respectively. The dark shaded band is the totally forbidden bandgap. The ligher shaded stripes above and below the dark band are forbidden only for s and p polarization respectively.

from which to view the Brillouin zone in Fig. 3a. Instead of having the f.c.c. BZ resting on one of its diamond-shaped facets as is usually done, we have chosen in Fig. 3a, to present it resting on a hexagonal face. Since there is a preferred axis for the atoms, the distinctive L-points centred in the top and bottom hexagons are three-fold symmetry axes, and are labeled L_3. The L-points centred in the other six hexagons are symmetric only under a 360° rotation, and are labeled L_1. It is helpful to know that the U_3-K_3 points are equivalent since they are a reciprocal lattice vector apart. Likewise the U_1-K_1 points are equivalent.

Normal incidence on the slab of Fig. 2 sends the propagation vector directly toward L_3 in reciprocal space ('the North pole'). Tilting the angle of incidence moves the propagation vector along a 'meridian' toward the 'equator'. By choosing different azimuthal angles toward which to tilt, the full reciprocal space can be explored. Fig. 3b shows the dispersion relations along different meridians for our primary experimental sample of normalized hole diameter $d/a = 0.469$ and 78% volume fraction removed. The oval points represent

experimental data with *s*-polarization ($\perp$ to the plane of incidence, $\parallel$ to the slab surface), while the triangular points represent p-polarization ($\parallel$ to the plane of incidence partially $\perp$ to the slab surface). The horizontal abscissa in the lower graph of Fig. 3b, L_3-K_3'-L_1-U_3-X-U_3-L_3 represents a full meridian from the North pole to the South pole of the BZ. Along this meridian the Bloch wave functions separate neatly into s and p polarizations. The *s* and *p* polarized theory curves are the solid and dashed lines respectively. The dark shaded band is the totally forbidden photonic bandgap. The lighter shaded stripes above and below the dark band are forbidden only for *s* and *p* polarization respectively.

Along the meridian L_3-W-K_1, the polarizations do not separate neatly, and only the totally forbidden photonic bandgap is shaded. The top of the valence band is at W and is mostly *s*-polarized, but the valence band maxima at U_3, X, and U_1 are almost as high. The bottom of the conduction band is at L_1, purely *p*-polarized, is only marginally lower than the valley at L_3. We have also measured the imaginary wave vector dispersion within the forbidden gap. At mid-gap we find an attenuation of 9 dB per unit cube length *a*. Therefore the photonic crystal need not be very many layers thick to effectively expel the zero-point electromagnetic field.

At a typical semiconductor refractive index, $n = 3.6$, and 3-d forbidden gap width is 19% of its centre frequency. We have repeated the calculation at lower refractive indices, re-optimizing the hole diameter. Our calculations indicate that the gap remains open for refractive indices as low as $n = 2.1$ using circular holes as in Fig. 2. In reactive ion etching, the projection of circular mask openings at 35° leaves oval holes in the material, which might not perform as well. Fortunately we found, defying Murphy's Law, that the forbidden gap width for oval holes is actually improved, fully 21.7% of its centre frequency.

In the visible region, there are many transparent optical materials available with a refractive index above 2.1. Furthermore, state-of-the-art reactive ion etching [15] can produce holes that are $\gtrsim 20$ times deeper than their diameter, deep enough to produce an f.c.c. photonic crystal with substantial inhibition in the forbidden gap. It appears that the application of photonic bandgaps to semiconductor physics, optical, and atomic physics may soon be practical.

3. Donor and acceptor modes

The photonic bandgap is very interesting in its own right. It is an energy band in which optical modes, spontaneous emission, and zero point fluctuations are all absent. Nevertheless, the photonic bandgap might actually be at its most interesting when the perfect translational symmetry is disrupted in a controlled manner. For example, by introducing a known degree of disorder, mobility edges and the Anderson localization transition [2] can be investigated.

Lasers, perhaps the most important application, also require that the 3-d translational symmetry should be broken. Even while spontaneous emission into all 4π steradians would be inhibited, a local electromagnetic mode is still necessary to accept the stimulated emission. In effect the local defect-induced structure resembles a Fabry–Perot cavity, except that it reflects radiation back upon itself in all 4π spatial directions. Meade *et al.* [16] have proposed that this could be accomplished by introducing a simple defect into the periodic geometry.

The perfect three-dimensional translational symmetry of a dielectric structure can be lifted in either one of two ways. (1) Extra dielectric material may be added to one of the unit cells. We find that such a defect behaves very much like a donor atom in a semiconductor. It gives rise to donor modes which have their origin at the bottom of the conduction band.

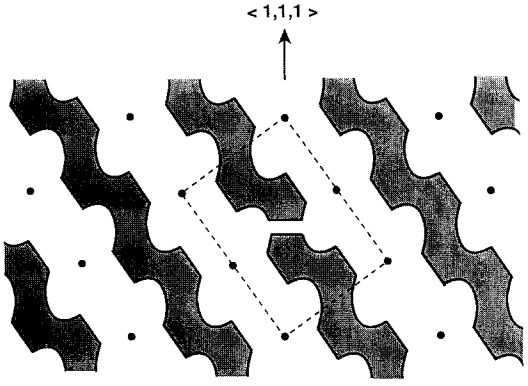

Figure 4 A $\langle 1, \bar{1}, 0 \rangle$ cross-sectional view of our face-centred-cubic photonic crystal [7] consisting of non-spherical 'air-atoms' centred on the large dots. Dielectric material is represented by the shaded area. The rectangular dashed line is a face-diagonal cross-section of the unit cube. Donor defects consisted of a dielectric sphere centred on an atom. We selected an acceptor defect as shown centred in the unit cube. It consists of a missing horizontal slice in a single vertical rib.

(2) Conversely, translational symmetry can be broken by removing some dielectric material from one of the unit cells. Such defects resemble acceptor atoms in semiconductors. The associated acceptor modes have their origin at the top of the valence band. We will find that acceptor modes are particularly well-suited to act as laser microresonator cavities. Indeed it appears that photonic crystals made of sapphire or other low-loss dielectrics, will make the highest-Q single-mode cavities (of volume $\approx 1\,\lambda^3$) covering all electromagnetic frequencies above the useful working range of superconducting metallic cavities. The short wavelength limit in the ultaviolet, is set by the availability of optical materials with refractive index $\gtrsim 2$, the threshold index [5, 7] for the existence of a photonic bandgap.

While the face-centred-cubic (f.c.c.) photonic crystal employing non-spherical atoms has already been fabricated [17] by reactive ion etching in GaAs, we have chosen to investigate local defect modes in larger structures on the scale of 1 cm wavelengths for now. We have introduced a single defect into our microwave photonic crystal. The 'doping' experiments are supplemented by theoretical calculations of the photonic bound states.

Photonic crystals generally consist of a continuous three-dimensional web of dielectric material, made up of inter-connecting ribs. The Wigner–Seitz unit cell of our photonic crystal [7] is the standard f.c.c. rhombic dodecahedron [7] with 'air-atoms' created by drill holes centred on the top 3 faces, which exit through the bottom 3 faces as shown in Fig. 1b. Figure 4 is a $\langle 1, \bar{1}, 0 \rangle$ cross-section of the same photonic crystal cutting through the centre of a unit cube. Shading represents dielectric material. The large dots are centred on the air-atoms and the rectangular dashed line is a face-diagonal cross-section of the unit cube. Such structures are made simply by drilling 3 sets of holes 35.26° off vertical into the $\langle 1, 1, 1 \rangle$ top face.

Since we could design the structure at will, donor defects were chosen to consist of a single dielectric sphere centred in an air-atom. Likewise, by breaking one of the inter-connecting ribs, it is easy to create acceptor modes. We selected an acceptor defect as shown in Fig. 4, centred in the unit cube. It comprises a vertical rib which has a missing horizontal slice.

The heart of this experimental apparatus is a 'doped' photonic crystal embedded in microwave absorbing pad as shown in Fig. 5. The photonic crystals were 8–10 atomic layers thick in the $\langle 1, 1, 1 \rangle$ direction. Cubic unit cell length was $a = 11$ mm and hole diameter was 5.16 mm, leaving an empty volume fraction $\approx 78\%$. Monopole antennas, consisting of 6 mm pins, coupled radiation to the defect mode. The HP 8510 network analyser was set up to measure transmission between the antennas. Figure 6a shows the transmission

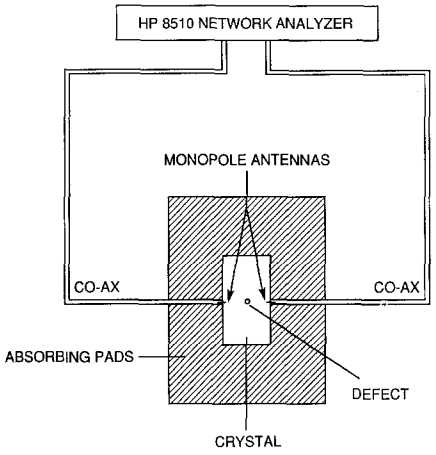

Figure 5 Experimental configuration for the detection of local electromagnetic modes in the vicinity of a lattice defect. Transmission amplitude attenuation from one antenna to the other is measured. At the local mode frequency the signal hops by means of the local mode in the centre of the photonic crystal, producing a local transmission peak. The signal propagates in the ⟨1, 1, 1⟩ direction through 8–10 atomic layers.

amplitude in the absence of a defect. There is very strong attenuation ($\approx 10^{-5}$) between 13 GHz and 16 GHz marking the valence and conduction band edges of the forbidden gap. This is a tribute to both the dynamic range of the network analyser, and the sizable imaginary wave-vector in the forbidden gap.

A transmission spectrum in the presence of an acceptor defect is shown in Fig. 6b. Most of the spectrum is unaffected, except at the electromagnetic frequency marked 'deep acceptor' within the forbidden gap. At that precise frequency, radiation 'hops' from the transmitting antenna to the acceptor mode and then to the receiving antenna. The acceptor level frequency, within the forbidden gap, is dependent on the volume of material removed. Figure 7 shows the acceptor level frequency as a function of defect volume removed from one unit cell. When a relatively large volume of material is removed, the acceptor level is deep as shown in Fig. 6b. A smaller amount of material removed results in a shallow acceptor level, nearer the valence band. If the removed material volume falls below a

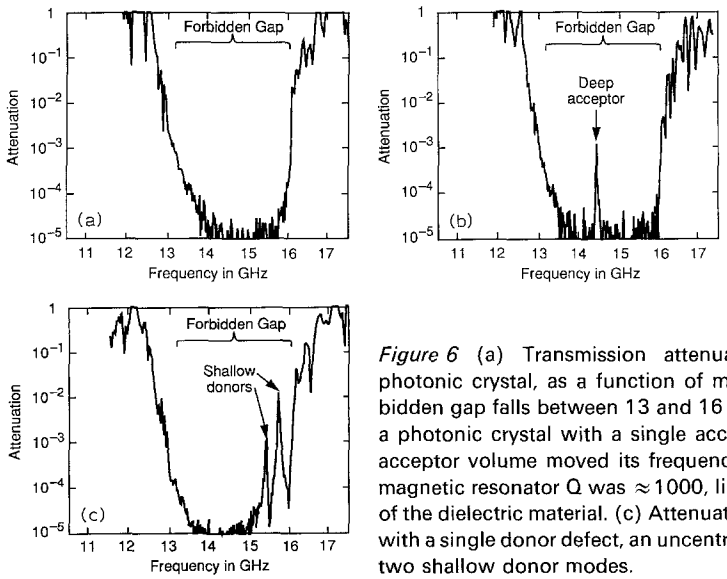

Figure 6 (a) Transmission attenuation through a defect-free photonic crystal, as a function of microwave frequency. The forbidden gap falls between 13 and 16 GHz. (b) Attenuation through a photonic crystal with a single acceptor in the centre. The large acceptor volume moved its frequency near mid-gap. The electromagnetic resonator Q was ≈1000, limited only by the loss tangent of the dielectric material. (c) Attenuation through a photonic crystal with a single donor defect, an uncentred dielectric sphere, leading to two shallow donor modes.

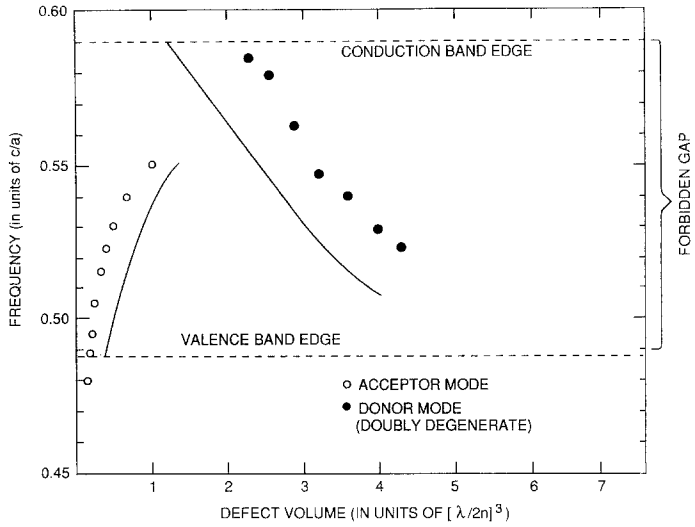

Figure 7 Donor and acceptor mode frequencies as a function of normalized donor and acceptor defect volume. The points are experimental and the corresponding lines are calculated. Defect volume is normalized to $[\lambda/2n]^3$ where λ is the mid-gap vacuum wavelength and n is the refractive index. A finite defect volume is required to bind a mode in the forbidden gap.

threshold volume, the acceptor level falls within the continuum of levels below the top of the valence band, becoming metastable.

On an expanded frequency scale we can measure the resonator Q of the deep acceptor mode, which is $Q \approx 1000$, as limited by the loss tangent of the Emerson & Cumming Stycast material of which the photonic crystal was made.

The behaviour of an off-centre donor defect is shown in Fig. 6c. In this case the donor volume was only slightly above the required threshold for forming bound donor modes. Already two shallow donor modes can be seen in Fig. 6c. When the donor is perfectly centred in the Wigner–Seitz unit cell, the two modes merge to form a doubly degenerate donor level as in Fig. 7. Single donor defects seem to produce multiple donor levels. Fig. 7 gives the donor level frequency as a function of donor volume. As in the case of acceptors, there is a threshold defect volume required for the creation of bound modes below the conduction band edge. However, the threshold volume for donor defects is almost ten time larger than the acceptor threshold volume. Apparently this is due to the electric field concentration in the dielectric ribs at the top of the valence band. Bloch wave functions at the top of the valence band are rather easily disrupted by the missing rib segment.

We have chosen in Fig. 7 to normalize the defect volume to a natural volume of the physical system, $(\lambda/2n)^3$, which is basically a cubic half-wavelength in the dielectric medium. More specifically, λ is a vacuum wavelength at the midgap frequency, and n is the refractive index of the dielectric medium. Since we are measuring a dielectric volume, it makes sense to normalize to a half-wavelength cube as measured at the dielectric refractive index. Based on the reasonable scaling of Fig. 7, our choice of volume normalization would seem justified. (Experimentally, the odd-shaped defect volumes were measured by weighing the samples).

It is interesting to compare our local modes to those of a one-dimensional Fabry–Perot

resonator, constructed in the usual manner of quarter-wave multilayer dielectric mirrors. In such a resonator the mirrors face each other and are usually separated by an integral number of half wavelengths. The net effect of the left and right mirrors facing each other is that they combine to form a monolithic 1-d periodic dielectric structure, but with a quarter wavelength of phase slip introduced into the very centre. This same quarter wavelength of phase slip is often employed in distributed feedback lasers [18], effectively converting them into Fabry–Perot resonators. The standing wave mode is sometimes [19] regarded as a bound state split off into the 1-d bandgap and localized to the quarter-wave defect in the periodic structure. In one dimension however, nothing requires that the defect be one-quarter wavelength long. A phase slip, no matter how small, allows a bound mode to form in the forbidden gap, usually near the band edge. This is in distinction to Fig. 7 where a finite-sized defect volume is required to bind a mode.

This is similar to the comparison between 1-d and 3-d quantum mechanics. In one dimension even an infinitesimal quantum well will bind [20] a state. In 3-d, a finite depth potential well is required to produce [20, 21] a bound state. Figure 7 is telling us that the same requirement for a finite defect volume applies to 3-d confined photon modes. John and Wang [6] have shown that the requirement for a finite volume-integrated polarizability can be satisfied even by a single resonant atom if undamped by non-radiative decay. Then an individual atom is capable of binding a local electromagnetic mode at its resonant transition frequency. They call this a photon-atom bound state. Inhibited spontaneous emission is accompanied with strong self-dressing of the atom by its own localized radiation fields, leading to anomalous Lamb shifts.

We have also performed calculations of the frequency spectrum of these dielectric systems. In order to solve for the electromagnetic modes, we expand Maxwell's equations in plane waves, employing the techniques of Ho *et al.* [5]. We employ the supercell method placing one defect in a repeated cell of dielectric material. Our calculations were performed in supercells containing eight f.c.c. Wigner–Seitz cells, and we have performed tests on larger supercells containing eight conventional f.c.c. cubic unit cells (32 Wigner–Seitz cells). Because the distance between defects is relatively small, there is significant overlap between the localized modes on neighbouring defects. This overlap manifests itself as a dispersion of the impurity band, and the frequency of the bound state is taken to be the band centre. We expanded the $\mathbf{H}(\mathbf{r})$ magnetic field in a basis of 4000 plane waves, and the lowest eigenvalues were obtained by the Vanderbilt [22] iterative diagonalization technique.

The solid lines in Fig. 7 show good qualitative agreement with the experimental points. The discrepancy between theory and experiment is larger for defects in supercells than for purely bulk systems, where better than 1% agreement has been achieved. There are two important reasons for this larger discrepancy. Firstly because of the larger unit cell size, it is necessary to work at a lower plane-wave cutoff. Second is the small number of primitive unit cells used in the supercell approximations. As in [16], the dispersion of the impurity band is quite large in the eight atom supercell, ≈ 20–80% of the gap-width for various states. Increasing the supercell to 32 atoms reduces the bandwidth by 80%.

4. Application to laser cavities

The extension of these 3-d dielectric microwave resonators to laser wavelengths is marked by the following considerations. The refractive index we have chosen to work with ($n = 3.6$) is a good match to the common semiconductors of which lasers are made. Furthermore, the f.c.c. geometry we are using has begun [17] to be microfabricated in GaAs.

Such micro-resonators will be particularly valuable for making tiny low-threshold lasers. But their value is greatly increased if the photonic bandgap inhibits spontaneous emission. In a semiconductor laser, this would lead to near unity quantum efficiency into the lasing mode. Photon number state squeezing [8] into that mode would be greatly enhanced. Inhibited spontaneous emission requires that the broad semiconductor luminescence band should be centred within the forbidden gap. In semiconductor lasers, population inversion and gain first appear at the red edge of the luminescence band, i.e. nearer to the valence band. This suggests that acceptor modes would be the appropriate defect type for lasers.

The other advantage for acceptor-mode laser cavities is associated with out acceptor defect geometry. The vertical rib with a missing horizontal slice, as in Fig. 4, can be readily micro-fabricated. It should be possible to create it in III–V materials by growing an aluminium-rich epitaxial layer and lithographically patterning it down to a single dot the size of one of the vertical ribs. After regrowth of the original III–V composition and reactive ion etching of the photonic crystal, HF acid etching, whose [23] selectivity $\geqslant 10^8$, will be used to remove the Al-rich horizontal slice from the one rib containing such a layer. The resonant frequency of the micro-cavity can be controlled by the thickness of the Al-rich sacrifical layer.

Acknowledgements

EY would like to thank Ho *et al.* [5] for telling about their diamond structure calculations before publication, and for intensive discussions of the degenerate Bloch wave functions at the W-point. John Gural deserves special thanks for his patience, dedication, and skilled machining of tens and thousands of holes, which made this project possible. KML's work is supported by ONR contract N00014-88-0500. The work at MIT was partially supported by ONR contract No. N00014-86-K-0158 and US JSEP contract No. DAAL-03-86-K-0002. RDM acknowledges valuable discussions with K. M. Ho.

References

1. E. YABLONOVITCH, *Phys. Rev. Lett.* **58** (1987) 2059.
2. S. JOHN, *Ibid.*, **58** (1987) 2486.
3. K. M. LEUNG and Y. F. LIU, *Ibid.*, **65** (1990) 2646.
4. Z. ZHANG and S. SATPATHY, *Ibid.*, **65** (1990) 2650.
5. K. M. HO, C. T. CHAN and C. M. SOUKOULIS, *Ibid.*, **65** (1990) 3152.
6. S. JOHN and J. WANG, *Ibid.*, **64** (1990) 2418.
7. E. YABLONOVITCH, T. J. GMITTER and K. M. LEUNG, *Ibid.*, **67** (1991) 2295.
8. Y. YAMAMOTO and S. MACHIDA, *Phys. Rev. A* **35** (1987) 5114.
9. E. YABLONOVITCH and T. J. GMITTER, *Phys. Rev. Lett.* **63** (1989) 1950.
10. S. SATPATHY, Z. ZHANG and M. R. SALEHPOUR, *Ibid.*, **64** (1990) 1239.
11. K. M. LEUNG and Y. F. LIU, *Phys. Rev. B* **41** (1990) 10188.
12. S. JOHN and R. RANGARAJAN, *Ibid.*, **38** (1988) 10101.
13. E. N. ECONOMU and A. ZDETSIS, *Ibid.*, **40** (1989) 1334.
14. E. YABLONOVITCH, unpublished.
15. A. SCHERER, B. P. VAN DER GAAG, E. D. BEEBE and P. S. D. LIN, *J. Vac. Sci. Technol.* **B8** (1990) 28.
16. R. D. MEADE, K. D. BROMMER, A. M. RAPPE and J. D. JOANNOPOULOS, published in *Phys. Rev. Rapid Communications.*
17. A. SCHERER and B. P. VAN DER GAAG, private communication.
18. H. KOGELNIK and C. V. SHANK, *J. Appl. Phys.* **43** (1972) 2328.
19. H. A. HAUS and C. V. SHANK, *IEEE J. Quantum Electron.* **QE-12** (1976) 532.
20. S. L. McCALL and P. M. PLATZMAN, *Ibid.*, **QE-21** (1985) 1899.
21. L. I. SCHIFF, 'Quantum Mechanics' (McGraw-Hill, New York, 1949) p. 37, 77.
22. R. NATARAJAN and D. VANDERBILT, *J. Comput. Phys.* **81** (1989) 218.
23. E. YABLONOVITCH, T. GMITTER, J. P. HARBINSON and R. BHAT, *Appl. Phys. Lett.* **51** (1987) 2222.